

# A NEW TYPE OF SPARK-PROTECTED PARALLEL MESH CHAMBER

P.Fonte<sup>(1,2)</sup>, N.Carolino<sup>(1)</sup>, L.Costa<sup>(3)</sup>, R.Ferreira-Marques<sup>(1,4)</sup>,  
S.Mendiratta<sup>(3)</sup>, V.Peskov<sup>(5)</sup>, A.Policarpo<sup>(1,4)</sup>

1-LIP, Dep. de Fisica, Univ. de Coimbra, 3000 Coimbra, Portugal.

2-ISEC, Quinta da Nora, 3000 Coimbra, Portugal

3-Departamento de Fisica, Univ. de Aveiro, 3800 Aveiro, Portugal.

4-Departamento de Fisica, Univ. de Coimbra, 3000 Coimbra, Portugal.

5-NASA Marshall Space Flight Center, Huntsville, AL 35812, USA.

## ABSTRACT

We developed a very low resistivity RPC-type detector, the anode of which was a plate made from materials with resistivity up to  $5 \times 10^7 \Omega \text{cm}$ , the cathode being a metallic mesh preceded by a drift region.

In such detector it was actually possible to combine the versatility and high counting-rate capability of metallic PPACs with the extreme robustness and "protectiveness" of Resistive Plate Chambers.

Occasional discharges triggered by large deposits of primary ionisation or by extreme counting rates are quenched by the resistive anode and are constrained to the glow discharge phase of the sparking process. The study shows that this discharge affects the detector only locally and the charge released is limited to a few tens of nC.

Proportional counting rates up to  $10^5 \text{ Hz/mm}^2$  were achieved at gains above  $10^4$ . The energy resolution at 6 keV was 20% FWHM. The observed gain-rate trade-off is well described by an analytic model and further improvements may be expected by lowering the resistivity of the anode material.

The properties of several custom-made, controllable resistivity, anode materials are described and perspectives of improvement in the performance of the detector are discussed.

## 1. Introduction

Parallel geometry chambers are used in three main configurations: Parallel Plate Chambers (PPCs), with two metallic electrodes, Resistive Plate Chambers (RPCs), with two resistive electrodes and Parallel Mesh Chambers<sup>1</sup> (PMCs), with multiple wire-mesh electrodes [1].

Common features of these detectors when operated in proportional mode are the good timing characteristics [2], good position resolution [3], easiness of production in large areas and large gain. The maximum gain is limited to the point where individual avalanches reach a charge around  $10^8$  electrons, triggering the formation of streamers [4] that subsequently evolve to higher current discharges [5]. Recently a new rate-induced breakdown mode was identified in PMCs [6].

In chambers with metallic electrodes (PPCs, PMCs) the discharge progresses until fully formed sparks appear. Although the sparks don't seem to affect the detector in a permanent way [7], the phenomenon causes unacceptable dead times and may compromise the integrity of the readout electronics.

When the electrodes are highly resistive (RPCs) the discharge is quenched at an earlier stage, affecting the detector only locally and being harmless to the readout electronics. It is even possible to operate the RPCs in a saturated gain "streamer mode", featuring very large and fast signals, up to a few hundred pC [8].

The advantage of RPCs in terms of sparkless operation is offset by a severe counting rate limitation of a few tens of  $\text{Hz}/\text{mm}^2$ , while PPCs and PMCs can reach counting rates at least up to  $10^5 \text{Hz}/\text{mm}^2$  [6,9] without any decrease of the pulse-height, suggesting their use as high-rate detectors.

It is attractive to attempt to combine the "protectiveness" of RPCs with the large counting rate capability of the metallic chambers. Earlier attempts [10] were focused on an asymmetric RPC with wire-mesh electrodes except for a resistive anode made of Pestov glass. However due to a lack of anode materials with lower resistivity, the counting rate of the device didn't exceed a few hundreds of  $\text{Hz}/\text{mm}^2$ .

In the present work we introduce a new custom-made medium resistivity material whose resistivity can be controlled from  $2 \times 10^7$  to  $3 \times 10^{12} \Omega \text{cm}$  allowing for a large flexibility in the chamber counting characteristics, while keeping essentially the same hybrid configuration described above.

---

<sup>1</sup> Also known historically as Parallel Plate Avalanche Chambers (PPACs), although in these detectors there are no plate electrodes.

The resulting detector actually combined the high counting-rate capability of PMCs ( $10^5 \text{Hz/mm}^2$ ) while keeping the extreme robustness and "protectiveness" of RPCs.

## 2. Experimental Setup

A schematic drawing of the experimental set-up can be seen in Fig.1. The detector was constituted by a drift region followed by an amplifying gap. The drift region was 15mm long and delimited by two wire meshes. The amplifying gap, 3.5mm long, was delimited by the lower drift mesh (cathode) and by a resistive plate (anode). The meshes were made of stainless steel wires of 50  $\mu\text{m}$  diameter placed at a pitch of 0.5mm. The detector had an active diameter of 4cm.

The primary charges were created by a collimated X-ray beam produced by a sharp-focus (0.1 mm) X-ray tube having a Fe anode. The tube produces a bremsstrahlung photon energy distribution peaked at 5.5keV with a maximum energy of 10keV. The beam was filtered by a nickel foil to absorb the lowest energy photons and delimited by a flat ring collimator placed 4cm from the tube anode, with selectable openings of 2 and 5mm diameter. The collimator was placed over the mylar entrance window, 1 mm from the upper drift mesh. It is estimated that the 5.5keV photons will generate 200 primary electrons, and this was the value used for all calculations.

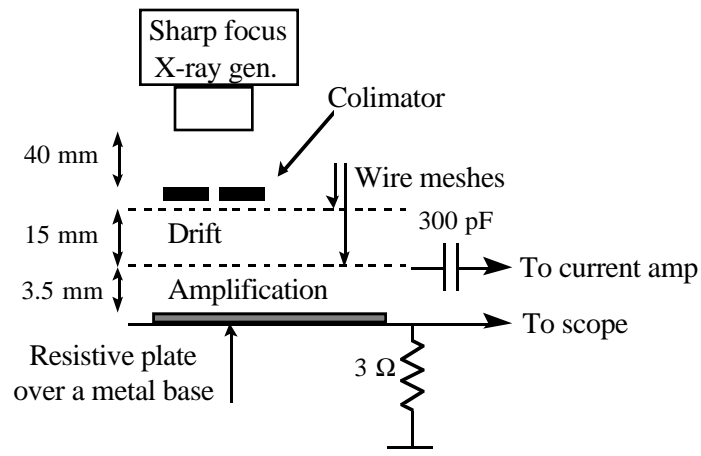


Figure 1 - Schematic representation of the experimental setup.

The resistive plate was deposited over a flat metal plate that provided mechanical support and an uniform electrical connection to the plate. The metal plate was grounded through a  $3 \Omega$  resistor and the current signal from discharges could be recorded directly on a scope connected in parallel with the grounding resistor.

The cathode signal was readout through a capacitor by a current amplifier with a 30ns rise time. Since the rise time of the amplifier was actually longer than the signal width, the pulse height at the amplifier output was related to the avalanche charge and not to the gap current. It was found that

the observed pulse shape at the amplifier output was well reproduced by injecting in parallel with the amplifying gap a square current pulse of 10ns width. When the amplitude was 160mA this pulse corresponded to the injection of  $10^7$  electrons or 1.6pC, thus providing a charge calibration of the readout system.

In order to measure the overall counting rate the output of the fast current amplifier was sensed by a discriminator whose trigger rate was measured by a time-windowed scaler. The peak noise level at the amplifier output was around 25fC and the discriminating threshold for all measurements was placed at 80fC. This relatively high level was forced by a noisy X-ray tube power supply.

If the resistive plate is considered in first approximation to be a purely ohmic conductor, a simple equivalent electrical circuit from the signal-source point of view can be derived (Fig.2). It can be calculated that the gap capacity per unit area is  $C_{gap}=0.25pF/cm^2$  and that the plate capacity per unit area is around  $C_{plate}=2.6pF/cm^2$  (assuming  $\epsilon_r=3$  and a plate thickness of 1mm). The total capacities can be estimated by multiplying those values by the plate area of  $25\text{ cm}^2$ . The value of the readout capacitor is  $C_{readout}=300pF$ .

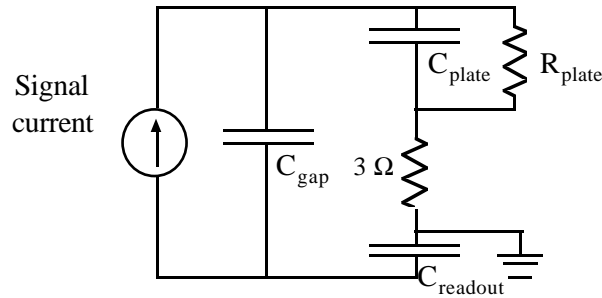


Figure 2 - Equivalent electrical circuit from the signal source (avalanche or streamer) point of view.

The gas mixture was constituted by Ar+20% $C_2H_6$  + methanol. The mixture was 50% saturated with the methanol vapours, that were required to prevent the resistive plate to become dry, with consequent increase of the plate surface resistivity.

### 3. Resistive material

The anodic resistive plate was made from a mixture of epoxy<sup>2</sup> and ink<sup>3</sup>, that yields a black rubber-like material.

<sup>2</sup> Araldite.

<sup>3</sup> MOLIN, ball-point pen black ink.

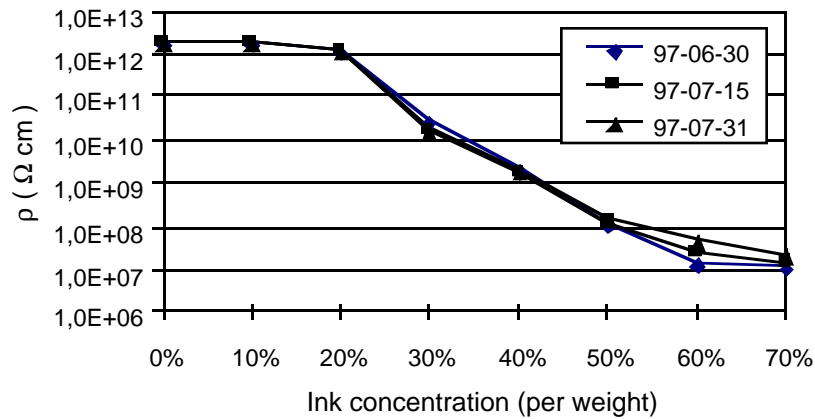


Figure 3 - The anodic material resistivity can be controlled by the amount of ink and varied from  $2 \times 10^7$  to  $3 \times 10^{12} \Omega \text{ cm}$ . Successive measurements taken at two weeks intervals suggest a good stability of the bulk resistivity.

The resistivity can be varied from  $2 \times 10^7$  to  $3 \times 10^{12} \Omega \text{ cm}$  by varying the ink concentration (Fig.3). Successive measurements taken at two weeks intervals suggest a good stability of the bulk resistivity.

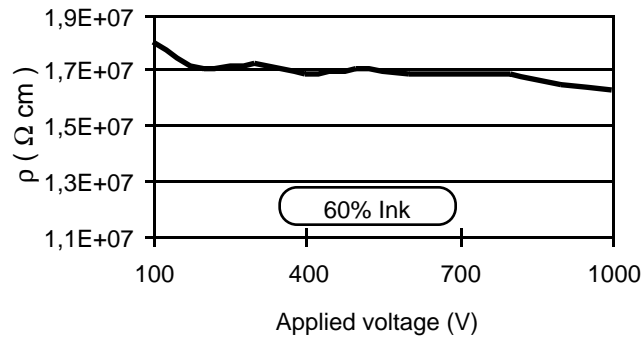


Figure 4 - The resistivity is largely independent from the applied voltage, indicating an ohmic behaviour.

The material shows an ohmic behaviour up to an applied voltage of 1kV (Fig.4) and, although there is some relaxation effect, the short term hysteresis cycle is quite narrow (Fig.5).

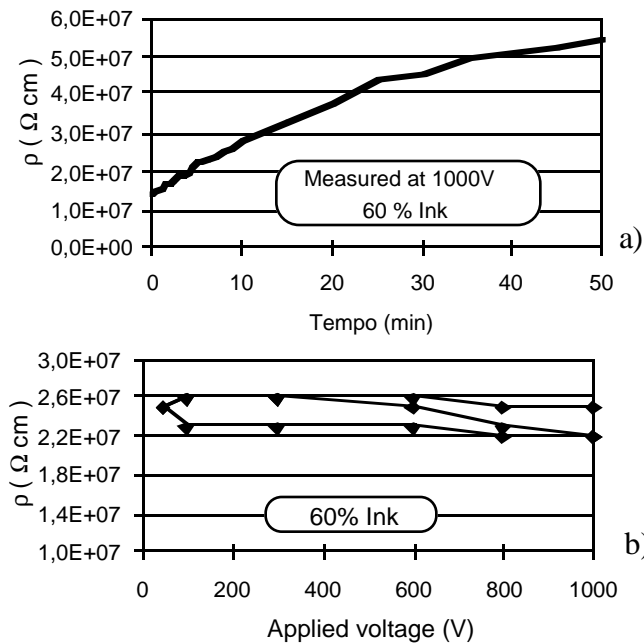


Figure 5 - Although the material shows a marked relaxation effect with a characteristic time of about 30 minutes (a), the fast cycling (1 minute per point) through large voltage excursions results on a relatively narrow hysteresis plot (b).

Further measurements have been performed in a systematic way, trying to identify materials of potential interest for this type of application. In particular Fig.6 shows results for melamine and for the above material, together with ABS plastic doped with  $\text{FeCl}_3$ . The latter seems to be a promising candidate, having much better mechanical characteristics than the epoxy-ink mixture. It is interesting to note the marked dependence of the resistivity with temperature

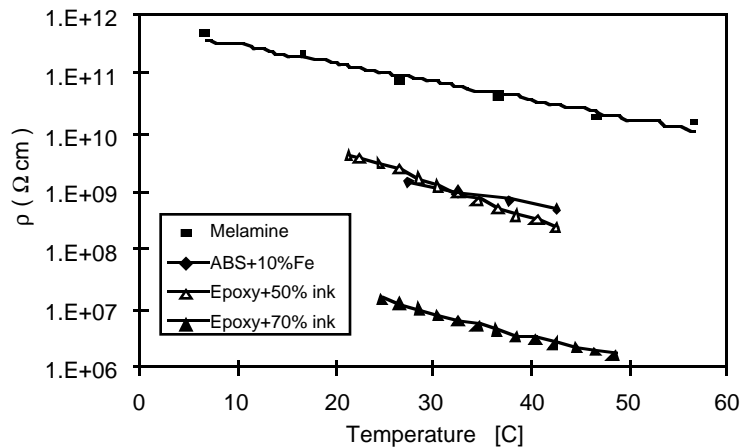


Figure 6 - Resistivity measurements performed for various materials in a temperature range of practical interest.

## 4. Results and Discussion

### 4.1 Counting Characteristics

The detector shows a reasonable energy resolution of 20% FWHM (Fig.7) for 5.9keV X-rays, while the best results for PMCs are typically around 14% FWHM [11]. In principle there is no reason why the present detector cannot achieve similar resolution values, so we attribute the observed reduced resolution to the deficient parallelism of the gap and to edge effects arising from the relatively small diameter of the active area.

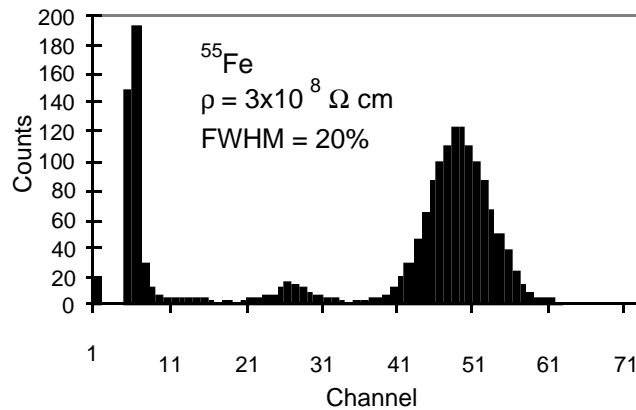


Figure 7 - A 20 % FWHM energy resolution was observed when the detector was illuminated by a  $^{55}\text{Fe}$  radioactive source emitting 5.9keV X-rays.

A large counting plateau of more than one order of magnitude in gain was observed when the detector was illuminated by 5.9keV X-rays (Fig.8). The corresponding dark current is negligible and sparks appear only at gains in excess of  $10^6$ . The dark current was found to be extremely sensitive to the presence of dust particles, requiring the detector to be assembled in a dust-free environment.

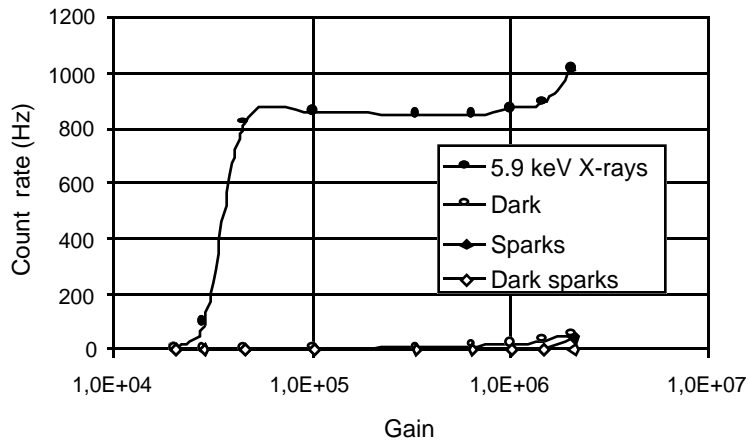


Figure 8 - A large counting plateau of more than one order of magnitude in gain was observed when the detector was illuminated by 5.9keV X-rays. The corresponding dark current is negligible and discharges appear only at gains in excess of  $10^6$ .

The gain-rate characteristics of the detector were studied for several combinations of applied voltages, plate materials and beam diameters, the detector being illuminated with X photons generated by the tube described in section 2. The results are shown in Fig.9.

For all plate materials, with resistivity ranging from  $4 \times 10^7 \Omega \text{cm}$  to  $4 \times 10^{11} \Omega \text{cm}$ , a reduction in gain for fixed applied voltage was observed above a certain rate threshold. The threshold rate is different for each plate, but seems to be relatively unaffected by the operating voltage or by the beam diameter.

For the lower plate resistivity studied, counting rates of  $10^5 \text{Hz/mm}^2$  were achieved at gains between  $10^4$  and  $10^5$ . This value is actually slightly above the intrinsic rate-gain limitations that were found in similarly built metallic PMCs [6], indicating that the optimum anode resistivity has been reached. The fact that in RPCs one can reach higher gains than in metallic chambers is well established in the literature, this fact being probably due to the “protectiveness” provided by the resistive electrodes.

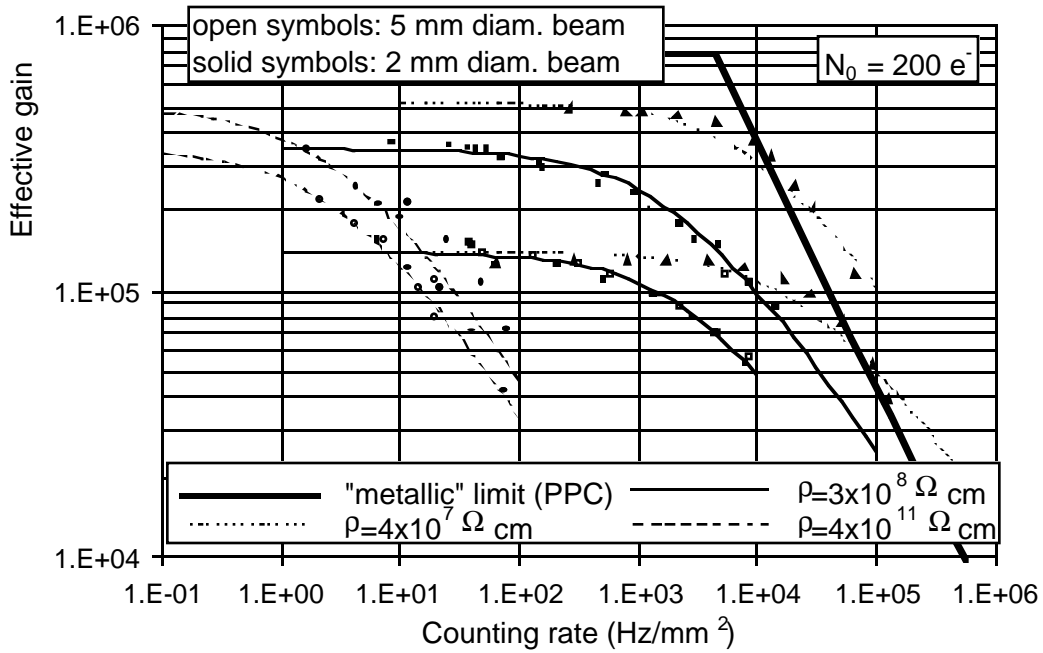


Figure 9 - Gain-rate characteristics of the detector for several values of the anode plate resistivity, beam diameters of 2 and 5 mm and two values of the applied voltage for each plate. For the lower resistivity studied counting rates of  $10^5 \text{ Hz/mm}^2$  were achieved at gains between  $10^4$  and  $10^5$ . The thin lines were adjusted according to the model described in the text and the thick solid line marks the experimentally determined intrinsic counting rate limitations of a similarly built all-metallic PMC [6].

#### 4.2 A Model of the Rate-Gain Dependence

The simplest assumption one can make about the origin of the rate-gain dependence is that it is caused by a reduction of the effective gap electric field owing to an ohmic voltage drop across the anode plate when crossed by the average avalanche current.

Mathematically the model can be expressed by the equations:

$$\begin{aligned}
 V &= V_0 - R I(V), \\
 R &= \rho \frac{L}{S} \quad I(V) = f e N_0 G(V), \\
 \frac{\ln G(V)}{d} &= A \exp\left(-\frac{B}{E}\right), \quad E = \frac{V}{d}, \quad (1)
 \end{aligned}$$

where  $V$  is the effective voltage across the gap,  $V_0$  is the applied voltage,  $I(V)$  is the gap current,  $R$  is the resistance seen by the gap current,  $r$  is the plate resistivity,  $L$  is the plate

thickness,  $S$  is the beam cross-section,  $f$  is the counting rate,  $e N_0$  is the primary charge,  $G(V)$  is the effective gain written in the Korff approximation and  $d$  is the gap length. The parameters  $A$  and  $B$  were determined experimentally for the gas mixture used.

The model relates the effective gap voltage  $V$  (as an implicit function) to the other quantities. Since the plate resistivity under the actual operating conditions is the most uncertain parameter of the model (actually immeasurable directly) it was chosen as a free parameter to be adjusted to the data.

The predicted rate-gain dependence was plotted in Fig.9 (thin lines). It can be seen that the model describes reasonably well the observed behaviour. Additionally, in table 1 the adjusted values of the plate resistivity are show for each curve and compared to the externally measured DC resistivity. The values agree within a factor of 2, seeming to validate the model when we consider that the range of resistivities covers 4 orders of magnitude and that the model doesn't take into account the beam-edge effects or the non-ohmic behaviour of the material.

	Externally	Adjusted	
	measured	$V_{01}$	$V_{02}$
$r$ ( $\Omega\text{cm}$ )	$4.0 \times 10^7$	$5.8 \times 10^7$	$3.8 \times 10^7$
	$3.8 \times 10^8$	$3.5 \times 10^8$	$1.8 \times 10^8$
	$4.1 \times 10^{11}$	$8.7 \times 10^{11}$	$6.1 \times 10^{11}$

Table 1 - Comparison between the values of the plate resistivity ( $r$ ) measured externally and the values estimated from the model after a least-squares adjustment to the data points show in figure 9 ( $V_{01}$  and  $V_{02}$  refer to the values of the applied voltage used for each plate). The resistivity values agree within a factor of 2, seeming to validate the model.

#### 4.3 Streamer charge

Discharges were triggered by streamers when the gain exceeded  $10^6$ , that is, when the avalanche charge exceeded  $2 \times 10^8$  electrons. Eventually some of the highest rate points shown in Fig.9 correspond to the limit of rate-induced breakdown [6], but this was not directly verified experimentally.

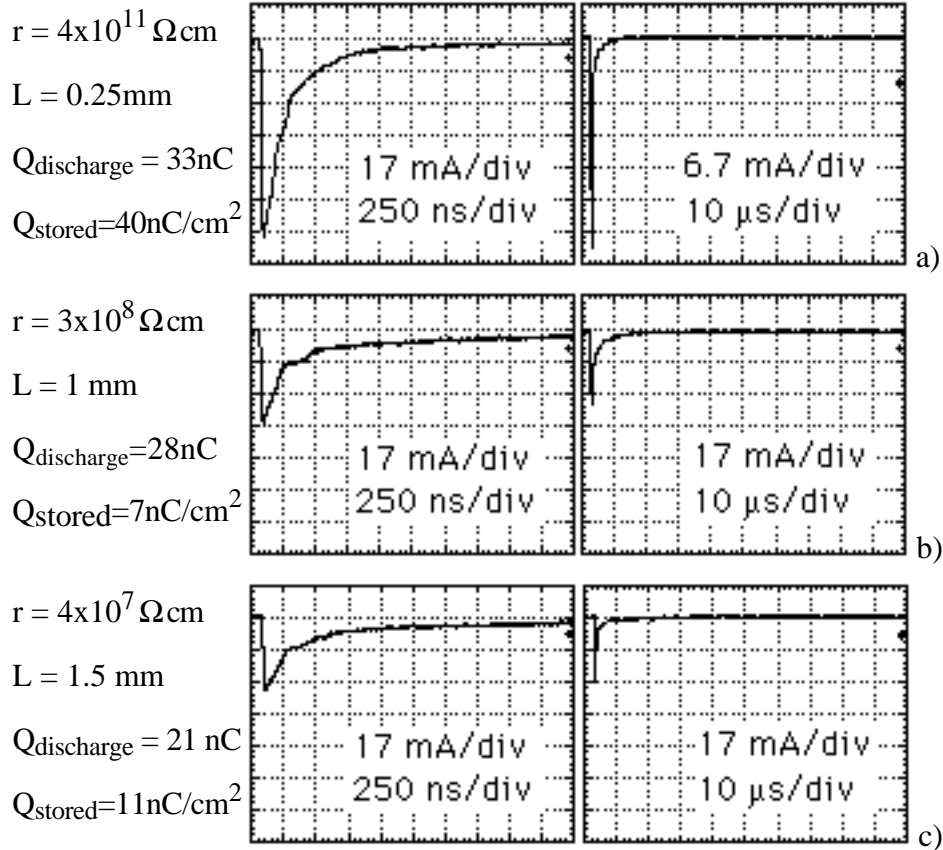


Figure 10 - Typical oscilograms of the discharge current for the anode plates studied in 2 different time scales. The quantities listed to the left of the oscilograms are: plate DC resistivity ( $r$ ), plate thickness ( $L$ ), observed discharge charge ( $Q_{\text{discharge}}$ ) and charge stored in the plate capacitor per unit area ( $Q_{\text{stored}}$ ).

As described in section 2, the discharge current could be observed directly on an oscilloscope, being a few typical oscilograms shown in Fig.10. The characteristics listed to the left of the oscilograms are: plate DC resistivity ( $r$ ), plate thickness ( $L$ ), observed discharge charge ( $Q_{\text{discharge}}$ ) and charge stored in the plate capacitor per unit area ( $Q_{\text{stored}}$ ). The discharge charge was estimated by integrating the area under the leftmost oscilogram for each plate and  $Q_{\text{stored}}$  was calculated from  $C_{\text{plate}}$  (see section 2) assuming a typical applied voltage of 4kV. From the values given in section 2 one can conclude that  $C_{\text{readout}} \gg C_{\text{plate}} \gg C_{\text{gap}}$  and from Fig.2 it can be seen that, from the capacitive point of view, the ratio between the charge transferred across the gap and the corresponding voltage change is dominated by  $C_{\text{plate}}$ .

For Fig.10a, ( $r = 4 \times 10^{11} \Omega \text{cm}$ ),  $Q_{\text{discharge}}$  is lower than  $Q_{\text{stored}}$ , corresponding to the release of the charge stored in a fraction of a  $\text{cm}^2$  of the plate surface.

For Fig.10b&c,  $Q_{discharge}$  is larger than  $Q_{stored}$  by a factor 2 to 3, suggesting that the conduction of current across the plate during the duration of the discharge is able to feed the discharge with an amount of charge at least comparable to the charge released from the plate surface.

Interestingly, the contribution to  $Q_{discharge}$  from conduction across the plate is not proportional to the measured DC plate resistivity ( $r$ ). This may be attributed to the fact that the discharge occurs in a short time (1ms), corresponding to a high-frequency voltage pulse applied to the plate, whose high-frequency resistivity may be completely different from the DC value.

#### 4.4 Type of Discharge

According to [5] the development of violent sparks in parallel geometry is preceded by a sequence of intermediate stages comprising the following discharge types: avalanche, streamer, glow discharge, filamentary discharge and spark.

In the present case the discharges were visually identified as being of the glow-discharge type, featuring a bright cathode spot at the apex of a faint conic-shaped glow region that extends up to the anode. It seems that the current restriction imposed by the anode material prevented the process to evolve beyond the glow-discharge stage.

For the lower resistivity material ( $r=4 \times 10^7 \Omega \text{cm}$ ) sometimes the glow discharge would be unquenched, fed by the conduction current across the plate. An increase in the amount of quencher ( $\text{C}_2\text{H}_6$ ) in the gas mixture strongly reduced the frequency of this phenomenon, without completely avoiding it. However it seems probable that the use of more efficient quenchers like isobutane or DME would further alleviate the problem.

## 5. Conclusions

We built and tested an asymmetric Resistive Plate Chamber able to achieve proportional counting rates up to  $10^5 \text{Hz/mm}^2$  at gains between  $10^4$  and  $10^5$ . The energy resolution at 5.9keV was 20% FWHM.

The chamber was constituted by an amplifying gap delimited by a resistive plate anode and a wire mesh cathode, preceded by a drift region. A new custom-made medium resistivity material was used for the anode plate, whose resistivity could be controlled from  $2 \times 10^7$  to  $3 \times 10^{12} \Omega \text{cm}$ .

Eventual discharges were quenched by the current limitation imposed by the resistive anode and constrained to the glow discharge phase of the sparking process. The discharge affected the detector only locally and the charge released was limited to a few tens of nC, independently of the plate DC resistivity.

The observed gain-rate trade-off is well described by a simple ohmic model.

Being the characteristic relaxation time of anodic plate ( $\tau$ ) of the order of a few ms, the electric transparency of the anode plate is preserved for the fast (<100 ns) electron signal. This will, in principle, allow a bidimensional strip readout to be placed below the anodic plate, with typical position resolutions of 100 to 200  $\mu$ m [3].

Finally, the spark protection concept presented here may be also useful when applied to higher-rate detectors like MICROMEGAS or other thin-gap parallel geometry chambers [12]. In such case, lower resistivity materials will be required and further research is therefore needed.

## 6. Acknowledgements

The authors gratefully acknowledge Crispin Williams and the LAA Project for lending some of the necessary hardware.

This work was done in the framework of the projects JNICT-CERN/P/FAE/1098/96 and JNICT-CERN/P/FAE/1143/97.

## 7. References

- [1] G.Charpak and F.Sauli, *Phys. Lett.*, 78B, pp.523, 1978.
- [2] E. Ceron Zebalos, *Sci. Acta XI-1*, pp.317, 1996  
A.Arefiev et al., *Sci. Acta XI-1*, pp.359, 1996  
M.Angelone et al, *Nucl. Instrum. Meth.* A355, pp. 359, 1995.
- [3] A. Peisert et al, *Nucl. Instrum. Meth.* A247, pp. 435, 1986  
E. Ceron Zebalos, *Nucl. Instrum. Meth.* A392, pp.150, 1997.
- [4] H.Raether, *Electron Avalanches and Breakdown in Gases* (London, Butterworths, 1964).  
J.M.Meek, in *Electrical Breakdown of Gases*, ed. J.A.Rees (London, MacMillan, 1973)  
P.Fonte et al., *Nucl. Instrum. Meth.* A310, pp.140, 1991  
P.Fonte, *IEEE Trans. Nucl. Sci.* vol.43, pp.2135, 1996.
- [5] S.C.Haydon, in *Electrical Breakdown of Gases*, ed. J.A.Rees (London, MacMillan, 1973).
- [6] Y.Ivaniouchenkov et al, “*The high rate behaviour of Parallel Mesh Chambers*”, presented at the 1997 IEEE Nuclear Science Symposium, 9-15 November, Albuquerque, New Mexico, USA, to be published in IEEE Transactions in Nuclear Science.
- [7] A.Arefiev et al., *Sci. Acta XI-1*, pp.359, 1996

- [8] I.Duerdoth et al, *Nucl. Instrum. Meth.* A348, pp.303, 1994  
R.Cardarelli et al, *Sci. Acta XI-1*, pp.11, 1996  
P.Fonte, *Sci. Acta XI-1*, pp.25, 1996
- [9] A.Peisert, *Nucl. Instrum. Meth.* 217, pp.229, 1983.  
J.Hendrix et al., *Nucl. Instrum. Meth.* A252, pp.246, 1986
- [10] V.Peskov et al, FERMILAB TM-1838, 1993  
D.F. Anderson et al, *Nucl. Instrum. Meth.* A348, pp.324, 1994
- [11] B.D.Ramsey et al, *Nucl. Instrum. Meth.* A248, pp.550, 1986
- [12] Y.Giomataris, *Nucl. Instrum. Meth.*, A376, pp.29, 1996.  
P.Fonte et al, "*Thin gap parallel mesh chamber: a sparkless high-rate detector*", preprint LIP/97-05, December 1997, (<http://xxx.lanl.gov/abs/physics/9803021>).